Carrier dynamics in InN nanorod arrays

Hyeyoung Ahn,[1,*] Chih-Cheng Yu,[1] Pyng Yu,[2] Jau Tang,[1,2] Yu-Liang Hong,[3] and Shangjr Gwo[3]

[1] *Department of Photonics and Institute of Electro-Optical Engineering, National Chiao Tung University, Hsinchu, 30010 Taiwan*
[2] *Research Center for Applied Sciences, Academia Sinica, Taipei, 115-29 Taiwan*
[3] *Department of Physics, National Tsing Hua University, Hsinchu, 30013 Taiwan*
[*] *hyahn@mail.nctu.edu.tw*

Abstract: In this report, we investigated ultrafast carrier dynamics of vertically aligned indium nitride (InN) nanorod (NR) arrays grown by molecular-beam epitaxy on Si(111) substrates. Dominant band filling effects were observed and were attributed to a partial bleaching of absorption at the probe wavelengths near the absorption edge. Carrier relaxation in nanorod samples was strongly dependent on the rod size and length. In particular, a fast initial decay was observed for carriers in NRs with a small diameter (~30 nm), the lifetime of which is much shorter than the carrier cooling time, demonstrating the substantial surface-associated influence on carrier relaxation in semiconductor nanostructures.

©2012 Optical Society of America

OCIS codes: (320.7150) Ultrafast spectroscopy; (160.4236) Nanomaterials; (300.1030) Absorption.

References and links

1. F. Chen, A. N. Cartwright, H. Lu, and W. J. Schaff, "Hole transport and carrier lifetimes in InN epilayers," Appl. Phys. Lett. **87**(21), 212104 (2005).
2. D. Zanato, N. Balkan, B. K. Ridley, G. Hill, and W. J. Schaff, "Hot electron cooling rates via the emission of LO phonons in InN," Semicond. Sci. Technol. **19**(8), 1024–1028 (2004).
3. J. W. Pomeroy, M. Kuball, H. Lu, W. J. Schaff, X. Wang, and A. Yoshikawa, "Phonon lifetimes and phonon decay in InN," Appl. Phys. Lett. **86**(22), 223501 (2005).
4. K. T. Tsen, J. G. Kiang, D. K. Ferry, H. Lu, W. J. Schaff, H.-W. Lin, and S. Gwo, "Electron-density dependence of longitudinal-optical phonon lifetime in InN studied by subpicosecond time-resolved Raman spectroscopy," J. Phys. Condens. Matter **19**, 236219 (2007).
5. T.-R. Tsai, C.-F. Chang, and S. Gwo, "Ultrafast hot electron relaxation anomaly in InN epitaxial films," Appl. Phys. Lett. **90**(25), 252111 (2007).
6. Y.-C. Wen, C.-Y. Chen, C.-H. Shen, S. Gwo, and C.-K. Sun, "Ultrafast carrier thermalization in InN," Appl. Phys. Lett. **89**(23), 232114 (2006).
7. R. Ascázubi, I. Wilke, S. Cho, H. Lu, and W. J. Schaff, "Ultrafast recombination in Si-doped InN," Appl. Phys. Lett. **88**(11), 112111 (2006).
8. S. Nargelas, R. Alecksiejunas, M. Vengris, T. Malinauskas, K. Jarasiunas, and E. Dimakis, "Dynamics of free carrier absorption in InN layers," Appl. Phys. Lett. **95**(16), 162103 (2009).
9. K. Fukunaga, M. Hashimoto, H. Kunugita, J. Kamimura, A. Kikuchi, K. Kishino, and K. Ema, "Energy- and density-dependent dynamics of photoexcited carriers in InN films," Appl. Phys. Lett. **95**(23), 232114 (2009).
10. H. Ahn, K.-J. Yu, Y.-L. Hong, and S. Gwo, "Carrier dynamics of Mg-doped indium nitride," Appl. Phys. Lett. **97**(6), 062110 (2010).
11. Y.-M. Chang and S. Gwo, "Carrier and phonon dynamics of wurtzite InN nanorods," Appl. Phys. Lett. **94**(7), 071911 (2009).
12. A. Othonos, M. Zervos, and M. Pervolaraki, "Ultrafast carrier relaxation in InN nanowires grown by reactive vapor transport," Nanoscale Res. Lett. **4**(2), 122–129 (2009).
13. H. Ahn, C.-H. Chang, Y.-P. Ku, and C.-L. Pan, "Free carrier dynamics of InN nanorods investigated by time-resolved terahertz spectroscopy," J. Appl. Phys. **105**(2), 023707 (2009).
14. H. Ahn, Y.-P. Ku, Y.-C. Wang, C.-H. Chang, S. Gwo, and C.-L. Pan, "Terahertz spectroscopic study of vertically aligned InN nanorods," Appl. Phys. Lett. **91**(16), 163105 (2007).
15. R. Calarco, M. Marso, T. Richter, A. I. Aykanat, R. Meijers, A. v.d. Hart, T. Stoica, and H. Lüth, "Size-dependent photoconductivity in MBE-grown GaN-nanowires," Nano Lett. **5**(5), 981–984 (2005).

#157961 - $15.00 USD Received 10 Nov 2011; revised 8 Dec 2011; accepted 11 Dec 2011; published 3 Jan 2012

16. C.-H. Shen, H.-Y. Chen, H.-W. Lin, S. Gwo, A. A. Klochikhin, and V. Yu. Davydov, “Near-infrared photoluminescence from vertical InN nanorod arrays grown on silicon: Effects of surface electron accumulation layer,” Appl. Phys. Lett. **88**(25), 253104 (2006).
17. A. A. Klochikhin, V. Y. Davydov, V. V. Emtsev, A. V. Sakharov, V. A. Kapitonov, B. A. Andreev, H. Lu, and W. J. Schaff, “Acceptor states in the photoluminescence spectra of n-InN,” Phys. Rev. B **71**(19), 195207 (2005).
18. R. P. Prasankumar, S. Choi, S. A. Trugman, S. T. Picraux, and A. J. Taylor, “Ultrafast electron and hole dynamics in germanium nanowires,” Nano Lett. **8**(6), 1619–1624 (2008).
19. R. P. Prasankumar, P. C. Upadhya, and A. J. Taylor, “Ultrafast carrier dynamics in semiconductor nanowires,” Phys. Status Solidi B **246**(9), 1973–1995 (2009).

1. Introduction

Indium nitride (InN) with a narrow direct band gap has superior electronic transport properties to other group-III nitrides so that InN has become attractive for various applications such as high-frequency electronic devices, near-infrared optoelectronics, and high-efficiency solar cells. With the rapid down-sizing of electronic and photonic device dimensions, better understanding of the carrier transportation in nanoscale matters is crucial. Several studies reported the carrier dynamics of the InN films [1–10] and its nanostructures [11, 12]. The time constant of hot carrier cooling in the InN film was measured to be in the range of subpicosecond to a few hundred picoseconds. The optical properties of low-dimensional semiconductors vary with their sizes and surface/environment interface properties, which can be different from those of bulk materials. Recently, by using the time-resolved terahertz transmission experiment, we measured the abnormally long carrier relaxation time in the InN nanorod (NR) arrays, which is attributed to the slow diffusion of carriers near the surface [13]. Carrier-carrier scattering time in InN NRs was considerably faster than that of InN epilayer [14].

Because of surface Fermi-level pinning, carriers in NRs with the rod diameter of the order of a depletion/accumulation layer experience the energy band deformation depending on the surface-to-volume ratio [15, 16]. Although the carrier relaxation in InN nanowires (NWs) was reported [12], its dependence on the rod size and the contribution of surface effect to the lifetimes of InN NRs remain unknown. In this paper, we performed optical-pump, near-infrared probe experiment on three NR samples and investigated the dependence of carrier dynamics on the rod height (*h*), diameter (*d*), and rod density. Transient reflectivity responses measured at near-IR probe wavelengths (1150 nm–1600 nm) and at different polarizations enabled us to understand various carrier absorption processes due to band filling (BF), band gap renormalization (BGR), and photoinduced absorption (PA). Results indicate that the absorption process of NR is dominated by the BF effect in contrast to the epilayer where the BGR effect is the main cause. The wavelength-dependent carrier lifetime is sensitive to the size of NRs. The carrier relaxation of the large-diameter (~120 nm) NR is similar to that of an epilayer, that is, fast cooling within ~2 ps followed by slow recombination. However, carriers in the small-diameter (~30 nm) NRs exhibited an additional initial decay that is faster than the cooling process. Strong polarization-dependent relaxation time is also observed for the 30 nm NRs, which demonstrates the anisotropy of absorption and relaxation along perpendicular and parallel direction to the axis of NR.

2. Experimental methods

Vertically-aligned InN NR arrays were grown on Si(111) substrates by plasma-assisted molecular-beam epitaxy (PAMBE). The InN nanorods were grown at a sample temperature of 520 þC on Si substrates and the rod density and diameter were controlled by means of the N/In ratio. For comparison of results, an InN epilayer was grown on Si(111) by using the epitaxial AlN/β-Si_3N_4 double-buffer layer technique. The epitaxial growth proceeded nominally under N-rich (N/In = 6.0) conditions, which resulted in the desired columnar morphologies. The details of growth method and conditions are described elsewhere [16]. Because the optical properties of NRs are dependent on the structural details of NRs, several InN NRs films with various rod heights and diameters were prepared and the detailed

#157961 - $15.00 USD Received 10 Nov 2011; revised 8 Dec 2011; accepted 11 Dec 2011; published 3 Jan 2012
(C) 2012 OSA

descriptions of samples used are listed in Table 1. The morphologies and size distribution of InN NRs were analyzed by using field-emission scanning electron microscopy (FE-SEM). The FE-SEM image of sample A in Fig. 1(a) indicates that most of the surface area of the film is covered by large-size NRs with *d*~143 nm and a smaller number of NRs with *d*~75 nm fill the gap between large NRs. For NRs with shorter height (= 240 nm) in Fig. 1(b), lateral growth of rod diameter was not apparent and the size distribution of NRs was uniform with an average diameter of NRs about 33 nm.

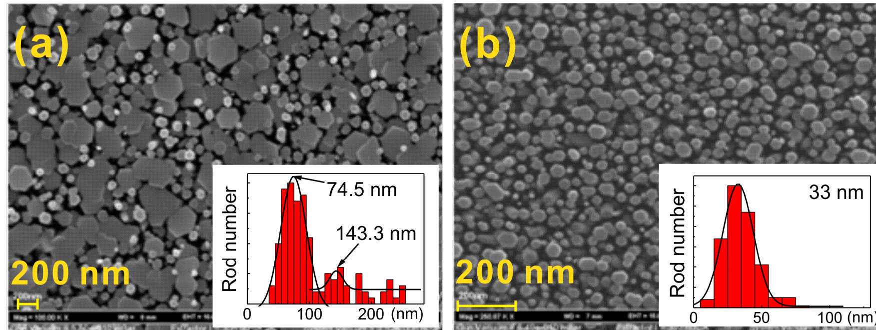

Fig. 1. FE-SEM image of the InN NRs with (a) the average height of 618 nm and the diameter of 87 nm and (b) the height of 240 nm and the diameter of 33 nm. Insets show the rod size distribution of the NR films.

The ultrafast pump-probe measurements were performed using an amplified Ti:sapphire laser system, which delivers ~50 fs optical pulses at 1 kHz repetition rate. The wide range of probe wavelength (λ) from 1150 nm to 1600 nm was obtained from an optical parametric amplifier system and strong 800 nm pump pulses were used to excite the InN NRs above the band gap, creating nonequilibrium electrons in the conduction band. The focused spot of the obliquely incident weak probe beam was maintained smaller than that of the pump beam and an optical chopper was used to improve the signal-to-noise ratio. The fluence of the 800 nm pump beam (F) was typically 2 mJ/cm^2.

Table 1. The details of InN NR film description [a]

Samples	Rods height (nm)	Average diameter (nm)	Total surface area occupied by NRs (%)	PL peak energy (eV)	Carrier density ($\times 10^{19}$ cm^{-3})
A	618	143/75	73	0.688	1.2
B	240	33	48	0.720	1.6
C	146	27	48	0.722	1.6

[a]The average diameter of nanorods is obtained from the rod size distribution plots shown in Fig. 1.

The variable-temperature PL spectroscopy was performed by using our femtosecond laser as the excitation source. The samples were cooled in a temperature-controlled liquid-He-flow cryostat. The luminescence signal was dispersed by a 0.19 m monochromator with a 600 groove/mm grating and detected by a liquid-N_2-cooled extended InGaAs detector (cutoff wavelength ≈2.4 μm). All the PL spectra have been corrected by the system response curve. Figure 2 shows normalized PL spectra from InN nanorods as well as an InN epitaxial film. The measured PL peak energy is 0.688 eV for sample A, 0.720 eV for sample B, and 0.722 for sample C. In comparison, the PL peak energy for the InN epitaxial film is 0.669 eV. The PL spectra indicate that the PL efficiencies of nanorod samples are about one order of magnitude lower than that of the InN epitaxial film. It was demonstrated previously that the electron concentration in *n*-InN samples can be estimated from fitting the line shapes of PL

#157961 - $15.00 USD Received 10 Nov 2011; revised 8 Dec 2011; accepted 11 Dec 2011; published 3 Jan 2012
(C) 2012 OSA

spectra [17]. Using this technique, the fitted electrons concentrations were found to be ~1.2 × 10^{19} cm^{-3} for sample A and ~1.6 × 10^{19} cm^{-3} for samples B and C.

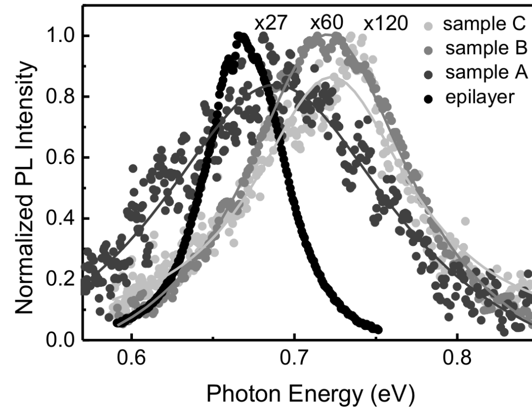

Fig. 2. Normalized photoluminescence spectra of an InN epitaxial film and three of nanorod samples A, B, and C. Solid lines are fitting curves with Lorentzian profiles. The peak energies of PL spectra are 0.669, 0.688, 0.720, and 0.722 eV for epilayer, sample A, sample B, and sample C.

3. Results and discussion

Time-resolved reflection transients ($\Delta R/R$) are shown in Fig. 3 for an InN epilayer and three NR samples A, B, and C excited with a pulse energy ~2 mJ/cm^2. For sample A in Fig. 3(b), the $\Delta R/R$ signals measured at the probe wavelengths (λ<1500 nm) sharply increase when the pump pulse arrives. The peak values of differential reflectivity $(\Delta R/R)_{\max}$ get smaller as the probing wavelength increases and beyond a critical probe wavelength (λ_c~1550–1600 nm) $\Delta R/R$ changes to a negative value. The initial rise/fall times of $\Delta R/R$ are pulsewidth-limited (~50 fs), which are much longer than the carrier-carrier scattering time (~15 fs) measured by the terahertz time-domain spectroscopy method [13]. Wavelength-dependent sign flip of $\Delta R/R$ of sample A contrasts to the response of $\Delta R/R$ of the InN film in Fig. 3(a), in which $\Delta R/R$ sharply decreases to a negative value for all probe wavelengths and the negative $(\Delta R/R)_{\max}$ increases in conjuction with the probe wavelength. For samples B and C, photoexcitation also results in an initial positive change in $\Delta R/R$; however no sign flip was observed at longer probe wavelengths. Relaxation of photoexcited carriers to equilibrium can be described by multiple exponential processes with characteristic lifetimes. Although the recovery of $\Delta R/R$ of epilayer film undergoes a biexponential decay with carrier lifetimes of τ_2, and τ_3, the transient $\Delta R/R$ signals of NRs recover with three time constants; τ_1, τ_2, and τ_3. Among them, τ_3 which governs carrier recombination is similarly long for both epilayer and NRs. The limit of our temporal scanning range prevents us from accurately determining τ_3 in our experiment, and here we focus on the carrier dynamics associated with the details of NRs. Therefore, Fig. 4(a) only shows fast carrier lifetimes τ_1 and τ_2. It is also necessary to clarify the possible contribution of Si substrate to $\Delta R/R$ signals. Under the same pump energy, the $\Delta R/R$ signals of bare Si substrates at the near-IR wavelength do not exhibit any temporal dependence. This result confirms that the $\Delta R/R$ responses presented in Fig. 3 are due to carrier dynamics in InN NRs.

#157961 - $15.00 USD Received 10 Nov 2011; revised 8 Dec 2011; accepted 11 Dec 2011; published 3 Jan 2012
(C) 2012 OSA

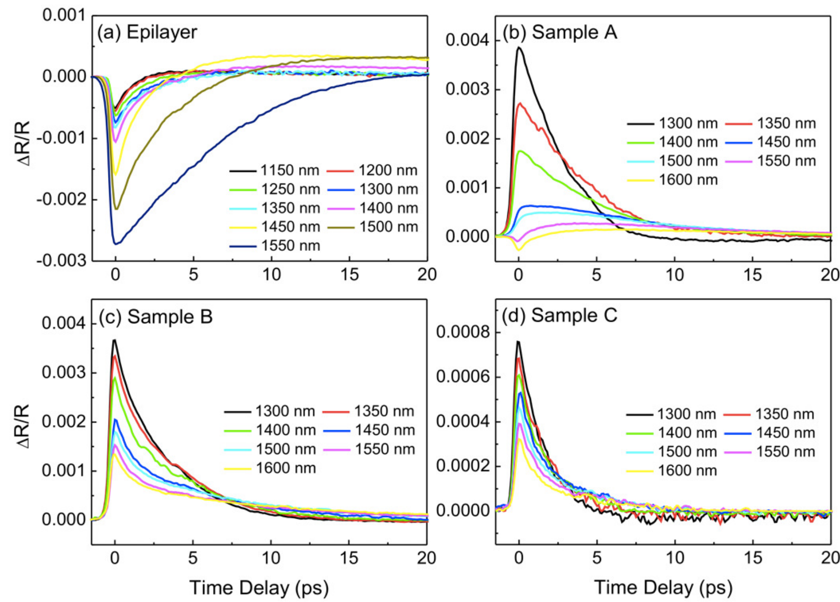

Fig. 3. Differential reflectivity transient of (a) InN epilayer and (b)-(d) NR samples A, B, and C measured at various probing wavelengths. Sample A with large rod diameter and long height has the sign flipping in $\Delta R/R$ as the probe wavelength increases beyond λ_c whereas sample B and C consisted of small diameter NRs have the positive change in $\Delta R/R$ for all probe wavelengths.

For photoexcited semiconductors, the transient reflectivity measured at various wavelengths exhibits the absorption and relaxation mechanisms. For high-density photoexcited carriers, the saturation of interband absorption causes bleaching of states at the absorption edge and strong screening of *e–h* Coulomb interaction leads to band gap shrinkage that is equivalent to an increase in the photon energy. Band gap renormalization influences the observed absorption process, because the photocarrier density of InN epilayer in our experiment is $>1 \times 10^{20}$ cm^{-3}, which is larger than the Mott carrier for InN [6]. Therefore, the large negative change of $\Delta R/R$ in InN epilayer, as shown in Fig. 3(a), can be attributed to the strong BGR effect. The increase of $(\Delta R/R)_{max}$ with the increase of probe wavelength and pump fluence [10] indicates that screening effect gets stronger near the bottom of conduction band where the effect of band gap renormalization is more significant.

The estimated background carrier density of the NR ($>10^{19}$ cm^{-3}) is much higher than that of epilayer (~3×10^{18} cm^{-3}), and a considerably larger negative change of $\Delta R/R$ can be expected because of stronger contribution of BGR. However, by contrast, Fig. 3 shows that the photoexcitation of InN NR leads to a sharp positive increase of $\Delta R/R$ and its maximal value $(\Delta R/R)_{max}$ decreases as the probe wavelength increases. Interestingly, $(\Delta R/R)_{max}$ for sample A becomes a negative value near λ~1550 nm. Previously, a similar sign flipping of $\Delta R/R$ has been observed for InN nanowires (NWs) near the interband absorption edge energy (E_a) [12]. The absorption edge energy is typically higher than the actual band gap energy because free electrons generated during the fabrication of the NWs occupy states near the bottom of the conduction band. Although it is much smaller than E_a (~1.52 eV) for NWs, we could estimate E_a~0.80 eV for sample A. Following the interband absorption, occupation of states in the conduction band which are normally unoccupied reduces the absorption and we attribute the positive transient behavior of $\Delta R/R$ of NRs to the bleaching of the absorption near the absorption edge. The bleaching caused by state filling decays as the hot carriers cool

#157961 - $15.00 USD Received 10 Nov 2011; revised 8 Dec 2011; accepted 11 Dec 2011; published 3 Jan 2012
(C) 2012 OSA

and relax to the bottom of the conduction band through carrier-phonon scattering. The $\Delta R/R$ signals will further decay as the excited carrier population near the surface is reduced by recombination and diffusion. Meanwhile, for samples B and C with 30 nm NRs, the $\Delta R/R$ signals in Fig. 3(c) and (d) show positive responses even at 1600 nm and the negative $\Delta R/R$ signals due to photoinduced absorption is not observed. The value of E_a is depicted by the density of free carriers associated with the growth of NRs and the additional injected carriers during photoexcitation. For 30 nm NRs, the small effective volume for absorption than that for large-size NRs and the presence of surface electron accumulation layer prevents the generation of high density photocarriers. In addition, narrower PL band of samples B and C than that of sample A in Fig. 2 indicates the growth of better quality NRs in samples B and C. As a result, E_a of sample B and C is smaller than that of sample A and it explains the positive $\Delta R/R$ signals in Fig. 3(c) and (d) due to the BF effect above the absorption edge.

Curve fits to the measured data indicate that the wavelength-dependent cooling time τ_2 for InN film is of the order of 2 ps, which is similar to those for samples A and C. Figure 4(a) shows that the cooling time of sample B is comparable, but is relatively longer than those of other samples, the reason for which remains unclear. Here, it is worthy to note that in addition to τ_2, samples B and C have an initial rapid decay time τ_1 which is in the range of 500 fs to 1 ps. Because samples B and C are consisted of the 30-nm NRs, τ_1 is expected to be strongly correlated with the carrier confinement in the small NRs. For InN, surface electron accumulation layer extends to approximately 10 nm below the surface. For samples B and C, the electron accumulation layer is comparable to the radius of NRs (~15 nm) and subsequently, the photoexcited carriers can be easily trapped by the surface-related defects with a short lifetime. A similar rapid decrease in the $\Delta R/R$ signal for small diameter nanostructure was also observed for Ge NWs [18]. Figure 4(b) shows the $\Delta R/R$ of sample B measured at various pump fluences. Inset in Fig. 4(b) exhibits the pump fluence dependence of carrier lifetimes τ_1 and τ_2. The carrier cooling time τ_2 increases linearly as F increases from 70 μJ/cm^2 to 2 mJ/cm^2 and the same fluence dependence was observed for other samples including InN epilayer [10]. Meanwhile, τ_1 decreases linearly with the increase of pump fluence, indicating that τ_1 is indeed associated with the carrier trapping by various defects and impurities near the nanorod surface and it gets shorter with the generation of high density photocarriers.

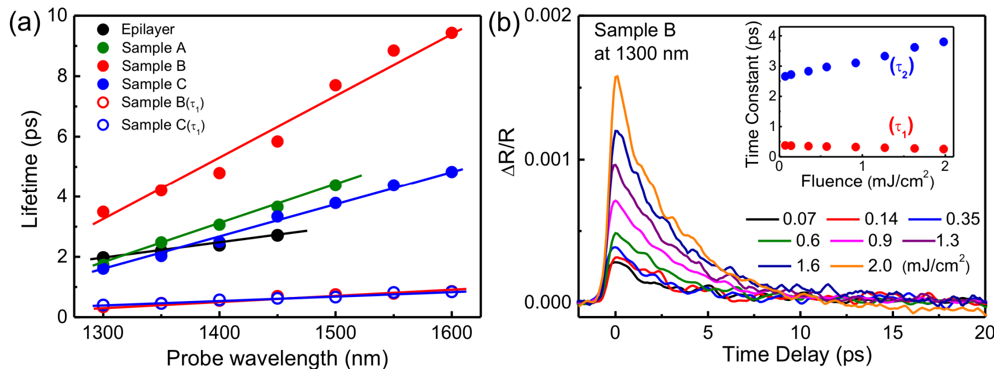

Fig. 4. (a) Carrier lifetimes of NR samples with different heights and diameters compared to that of epilayer film. Solid symbols represent the carrier cooling times and open circles are the rapid initial decay time observed for samples B and C. Slow recombination time constants are not shown here. (b) Pump fluence dependence of differential reflectivity transient of sample B. Inset shows the carrier lifetimes τ_1 and τ_2 at the corresponding pump fluences.

For NRs, large dielectric mismatch between the NR and its surrounding material causes the polarization of absorption within the NR; consequently, the perpendicular component of absorption to the axis of NR is strongly suppressed compared to the parallel component [19].

#157961 - $15.00 USD Received 10 Nov 2011; revised 8 Dec 2011; accepted 11 Dec 2011; published 3 Jan 2012
(C) 2012 OSA

Carrier dynamics parallel and perpendicular to the axis of NR is investigated by measuring $\Delta R/R$ with *s*- and *p*-polarized 1500 nm probe beams. Figure 5 demonstrates that for sample B, the *s*-polarized component of $\Delta R/R$ decays more rapidly than that of *p*-polarized component, whereas both polarization components decay in a similar way for sample A. This suggests that carriers propagating perpendicular to the axis of NR are rapidly trapped or recombined at the surface, while carriers propagating parallel to the axis of NR travel much longer distance before trapping or recombination. The anisotropy of decay time depends on the diameter-to-height (*d/h*) ratio of NR. The inset of Fig. 5(b) illustrates the polarization dependence of decay time for sample C. Although sample C has the same rod diameter as sample B, the difference in its decay time between *s*- and *p*-polarized components is substantially smaller than that of sample B, which may be attributed to larger *d/h* ratio of sample C than that of sample B.

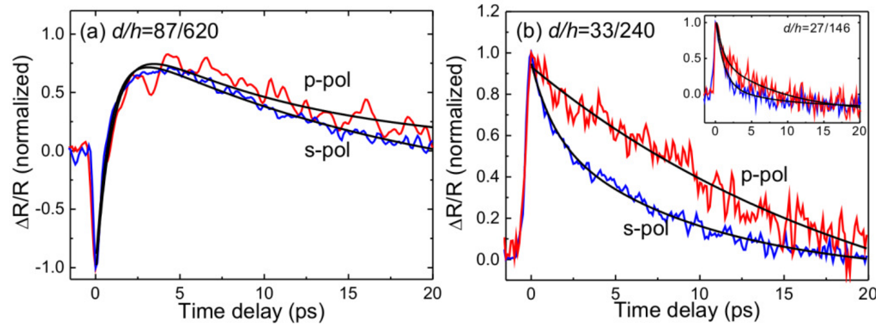

Fig. 5. Polarization dependence of differential reflectivity transient of (a) sample A and (b) sample B measured at the pump fluence of 2.2 mJ/cm^2. The initial fast drop of reflectivity followed by the positive signal in (a) indicates the competition of absorption processes near the interband absorption edge energy. Inset in (b) shows the polarization dependence of $\Delta R/R$ of sample C, which has smaller *d/h*.

4. Summary

In summary, we demonstrated the probe wavelength-dependent carrier transport dynamics in vertically aligned InN nanorod arrays. Bleaching of those states near the absorption edge was commonly observed for all nanorod samples with various nanorod heights and diameters and is directly contrasted with band gap renormalization-dominant absorption process of epilayer. Carriers in large-diameter nanorods were found to relax to the equilibrium in a similar way to that in an epilayer film, but carriers in 30 nm nanorods were found to be quickly trapped by the surface much faster in a time scale than the carrier cooling and recombination times.

Acknowledgement

This work was supported in part by the National Science Council, Taiwan through the National Nanoscience and Nanotechnology Program (Grant No. NSC-99-2120-M-007-004) and a research project (Grant No. NSC-99-2112-M-009-MY3).